

**Summertime inter-annual temperature
variability in an ensemble of regional model
simulations:
analysis of the surface energy budget**

*G. Lenderink, A. van Ulden, B. van den Hurk and
E. van Meijgaard*

De Bilt, 2006

PO Box 201
3730 AE De Bilt
Wilhelminalaan 10
De Bilt
The Netherlands
<http://www.knmi.nl>
Telephone +31(0)30-220 69 11
Telefax +31(0)30-221 04 07

Author:
Lenderink, G.
Ulden, A. van
Hurk, B. van den
Meijgaard, E. van

Summertime inter-annual temperature variability in an ensemble of regional model simulations: analysis of the surface energy budget

G. Lenderink, A. van Ulden, B. van den Hurk and E. van Meijgaard

KNMI Scientific Report

June 2006

In autumn 2005 this paper has been accepted for publication in the special issue on the PRUDENCE project in Climatic Change by the coordinators of the special issue. However in spring 2006 it turned out that there were significant page limitations for the special issue imposed by Climatic Change. Therefore, the original manuscript had to be revised in order to reduce its length considerably. This scientific report acts to document this work in its original, unabridged form. The appendix contains additional material which was not contained in the original paper.

Summertime inter-annual temperature variability in an ensemble of regional model simulations: analysis of the surface energy budget

G. Lenderink, A. van Ulden, B. van den Hurk, and E. van Meijgaard
Royal Netherlands Meteorological Institute

August 26, 2005 (revised version)

Abstract. The inter-annual variability in monthly mean summer temperatures derived from nine different regional climate model (RCM) integrations is investigated for both the control climate (1961-1990) and a future climate (2071-2100) based on A2 emissions. All regional model integrations, carried out in the PRUDENCE project, use the same boundaries of the HadAM3H global atmospheric model. Compared to the CRU TS 2.0 observational data set most RCMs (but not all) overpredict the temperature variability significantly in their control simulation. The behaviour of the different regional climate models is analysed in terms of the surface energy budget, and the contributions of the different terms in the surface energy budget to the temperature variability are estimated. This analysis shows a clear relation in the model ensemble between temperature variability and the combined effects of downward long wave, net short wave radiation and evaporation (defined as F). However, it appears that the overestimation of the temperature variability has no unique cause. The effect of short-wave radiation dominates in some RCMs, whereas in others the effect of evaporation dominates. In all models the temperature variability increases when imposing future climate boundary conditions, with particularly high values in central Europe. The surface energy budget analysis again shows a clear relation between changes in F and the change in temperature variability.

Keywords: PRUDENCE, model physics, inter-quartile range

1. Introduction

The summer of 2003 has been excessively warm in large parts of Europe with monthly mean temperatures in central Europe exceeding the previous observed maximum by two degrees or more (Schär et al., 2004; Luterbacher et al., 2004; Beniston and Diaz, 2004). Schär et al. (2004) estimated the chance that these high temperatures would occur under present-day climate conditions to be extremely low. They presented results of a regional climate model (RCM) integration, which predict that the mean temperature as well as its inter-annual variability will increase compared to the present-day conditions. They concluded that an increase of the variability of the summertime temperatures could drastically increase the probability of extremely warm summer events, and hypothesize that the 2003 summer conditions might be a manifestation of this effect.

Temperature variability is determined by combined effects of the large-scale atmospheric circulation and small-scale physical processes, like long wave and

Table I. The regional climate models

Institute	Model	Model reference
DMI	HIRHAM	(Christensen et al., 1996)
ETHZ	CHRM	(Vidale et al., 2003)
GKSS	CLM	(Steppeler et al., 2003)
METO	HadRM3H	(Hulme et al., 2002)
ICTP	RegCM	(Giorgi and Mearns, 1999)
KNMI	RACMO2	(Lenderink et al., 2003)
MPI	REMO	(Jacob, 2001)
SMHI	RCAO	(Räsänen et al., 2004)
UCM	PROMES	(Sanchez et al., 2004)

short wave radiation, boundary-layer turbulence and soil processes determining latent and sensible heat fluxes. In atmospheric models, these smaller scale physical processes are parameterized by cloud, radiation, soil and turbulence schemes. As such, these parameterization schemes exert a strong control on the temperature variability. For example, a soil scheme that is sensitive to drying may lead to high temperature in summer (Seneviratne et al., 2002). Although there is ample literature about these processes in individual models (Räsänen et al., 2004; Vidale et al., 2003; Giorgi et al., 2004), no comprehensive summary of how they operate in a suite of models exists to date.

In the European project PRUDENCE (Prediction of Regional scenarios and Uncertainties for Defining European Climate change and Effects, Christensen et al., 2002) nine different RCMs are used to simulate both present-day climate (1961-1990) and future climate (2071-2100) assuming an SRES A2 emission scenario. These simulations are all driven by the same boundaries, which approximately enforce the same statistics of the large scale dynamics in the model domain (Van Ulden et al., 2005). Therefore, this ensemble provides an ideal testbed to analyse the impact of the physics parameterizations on the model behavior, and in particular on the simulated temperature variability. As a first step in this process, we consider in this study differences in the simulated surface energy budget (as determined by the model physics) and relate these to the differences in summertime temperature variability. In Vidale et al. (2005) the relation between soil moisture and temperature variability is studied in the same PRUDENCE model ensemble.

2. Temperature variability compared to observations

In the framework of the European project PRUDENCE nine different RCMs were used to downscale global simulations of the atmospheric model HadAM3H

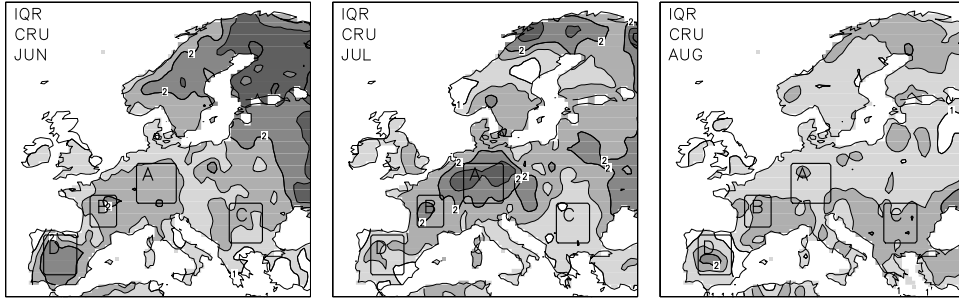


Figure 1. Interquartile range (IQR) of the monthly mean temperature in the CRU observations for June, July, and August. Shading interval $0.5\text{ }^{\circ}\text{C}$. Also shown are four different areas: GER (A), SFRA (B), SEU (C), and SPA (D)

performed for the present-day climate 1961-1990 and a future climate 2071-2100 using the SRES A2 emission scenario (Jones et al., 2001). The RCMs (see Table 1) differ with respect to the physics parameterization packages and the implementation of the atmospheric dynamics, although some models share the same dynamical core (e.g. RCAO and RACMO2). All RCMs cover most of Europe with an approximate resolution of 50 km, but the central location and size varies to some extent between the different models; e.g. the RegCM and PROMES have their northern boundary of the domain in central Scandinavia. From the available RCMs integrations monthly mean output was obtained from the PRUDENCE data base (<http://prudence.dmi.dk>). The temperature time series of the future climate integration (2071-2100) are detrended using the trend over that period in HadAM3H over the northern hemisphere ($2\text{ }^{\circ}\text{C}$ over 30 years). This detrending has a small impact (compared to the climate change signal) on the computed values for the temperature variability.

The RCM output is compared to the Climate Research Unit (CRU) TS 2.0 observational time series of monthly means (period 1961-1990) on a regular 0.5×0.5 degree lat-lon grid (New et al., 2000). The RCM output has been interpolated from the native model grid to the CRU grid. As a measure of the variability the inter-quartile range (IQR) (between the 25% and 75% quantiles) is considered for each summer month. For the CRU observations results are shown in Fig. 1. In general, the temperature variability is largest in June, and smallest in August, with the exception of central Germany and France where the temperature variability is largest in July. For most areas the inter-quartile range is about $1.5 - 2.5\text{ }^{\circ}\text{C}$ for all summer months, with the lowest values for August. Figure 1 also shows four different areas used for further analysis: Southern France (SFRA), Germany (GER), Spain (SPA) and Southeastern Europe (SEU). For the RCMs and the driving HadAM3H simulation the difference with the CRU observations is shown in Fig. 2.

The HadAM3H results (Fig. 2 left panels on top) show reasonably small deviations from the CRU observations during early summer in June (except

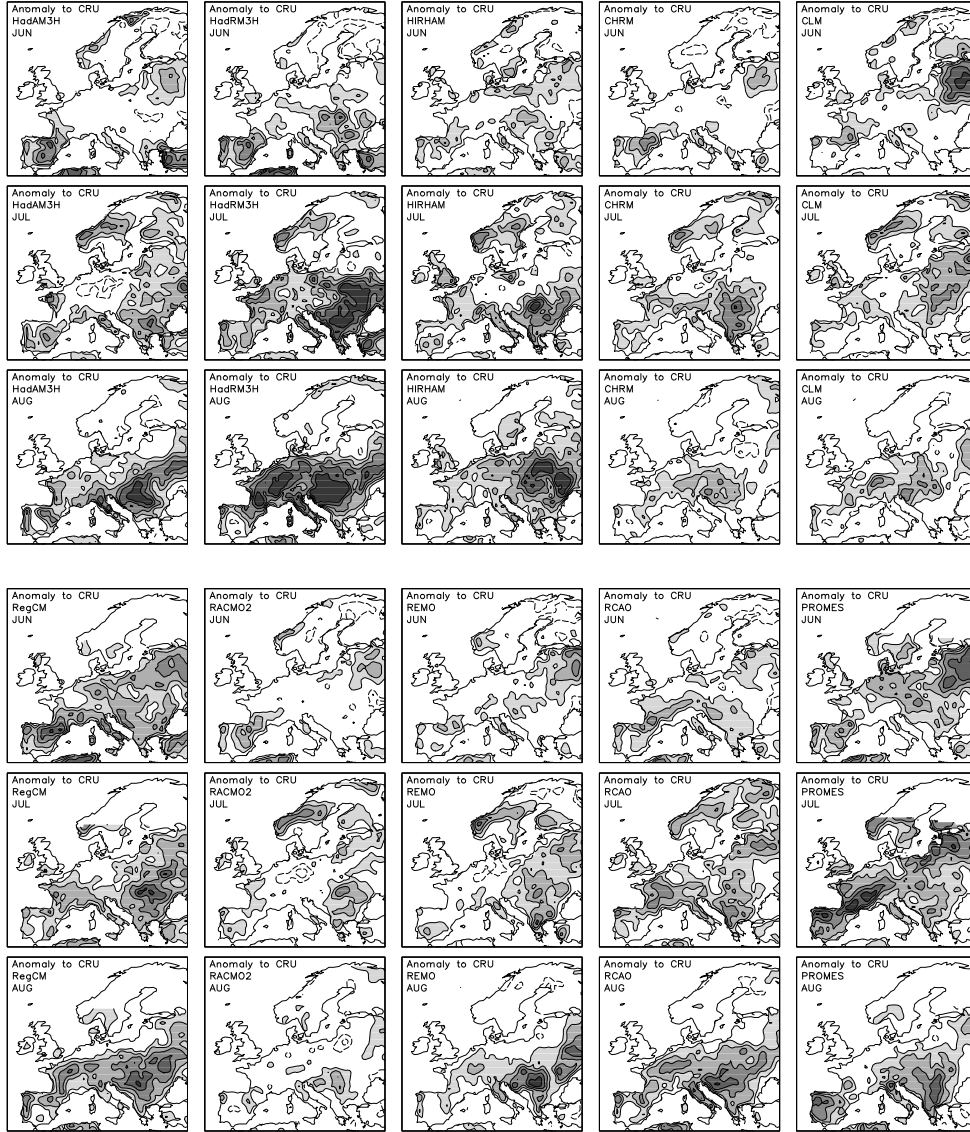


Figure 2. IQR of the monthly mean temperature in HadAM3H and the RCM ensemble. Shown are deviations from the observations (CRU). Shading starts at 0.5 °C with steps of 0.5 °C. Dashed contours denote negative values below -0.5 °C.

in Spain). In August, and to a lesser extent in July, the deviations are larger, typically 1-2 °C overestimation of the IQR in large parts of central and eastern Europe.

The outcome of the regional models show a large spread around the HadAM3H results; some models are clearly closer to the observations while others are deviating more. The temperature variability in RACMO2, CLM, CHRM, and

REMO is (rather) close to the observations, but the majority of the models overpredict the IQR in central (including France) and southeastern Europe, up to more than 2 degrees (100 %) in HadRM3H, PROMES and RegCM. For this area some models show a clear increase in variability during the course of the summer (HadRM3H, HIRHAM, and to a lesser extend RCAO and REMO), suggesting that progressive soil drying during summer plays a role. In particular striking is the large increase in variability from the HadAM3H global simulation to the regional HadRM3H simulation, considering that both models essentially share the same model physics. Further analysis (not shown) revealed that most models overestimate the temperatures in the high tail of the distribution, with the exception of PROMES and CLM which underestimate temperatures in the low tail.

3. Evaporation and radiation

3.1. MEAN FLUXES

Mean fluxes of evaporation and net short-wave radiation at the surface are shown in Fig. 3 for two areas, GER (relatively wet and cloudy) and SPA (dry and sunny). Evaporation is used here for the total evaporation from the surface, including transpiration from the vegetation, which is (in hydrological sciences) commonly denoted as evapotranspiration. For both evaporation and short wave radiation, the spread in the model ensemble is considerable. We note that, in general, there appears to be a (small) compensation between shortwave radiation and evaporation with models with high surface radiation tending to have large evaporation rates, and vice-versa. This might partly be a consequence of the way models are tuned, since high (low) surface insolation, leading to high surface temperatures, may (to some extent) be compensated by high (low) evaporation rates. Conversely, cloud radiative properties and thereby surface insolation may also be adjusted to compensate for anomalous evaporation rates. While such tuning may be successful for the simulation of the mean temperature, it may also have important implications for the simulated temperature variability. For example, the low mean value of radiation in PROMES suggests a strong cloud-radiation control, which also appears to impact on the simulated temperature variability in that model (as will be shown in the next sections).

Net short wave fluxes in the model ensemble are about 60 Wm^{-2} lower and evaporation rates are about 40 Wm^{-2} higher in GER than in SPA. Evaporation is determined by drying capacity of the atmosphere (often measured by the potential evaporation) restricted by limitations imposed by the dryness of the soil. Potential evaporation is strongly linked to the amount of net short wave radiation at the surface, which is larger in SPA than in GER, and therefore soil water depletion plays a larger role in SPA than in GER. The reduction of

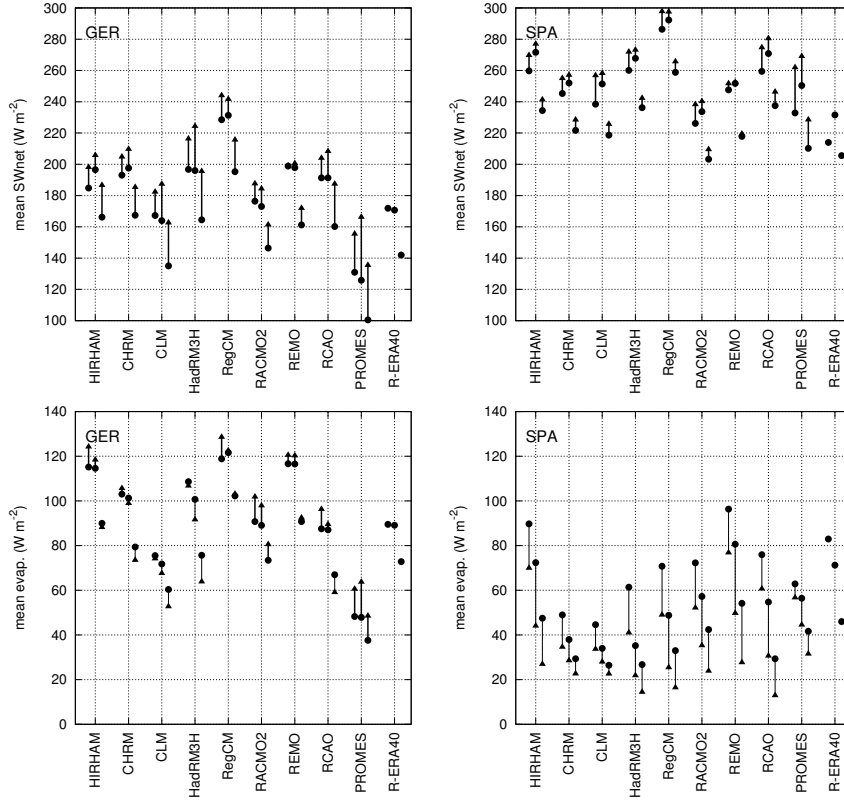


Figure 3. Mean net short-wave radiation and evaporation for GER and SPA. For each RCM results for June, July and August (three consecutive symbols/lines) are shown. Solid dots (triangles) are results for the control (future) integration, with a thick (thin) line denoting increase (decrease) from control to future simulation.

evaporation during summer in SPA also is caused by the progressive drying of the soil. Results for SFRA and SEU are in between (not shown).

3.2. METHOD OF ANALYSING VARIABILITY

To analyse the relation between surface fluxes and temperature, we define an “average” difference in the surface flux (e.g. in evaporation) that is related to the temperature variability as follows. First, for each area and each summer month, we sorted the 30-year time series of the monthly-mean, area-mean temperature. Figure 4 shows a quantile plot of such sorted temperatures for August in GER. At the same time we ordered the surface energy flux using the temperature as sorting criterion. For the same month and area, the co-sorted data for short-wave radiation and evaporation is plotted in Fig. 4. (Note that for a particular model one position on the x-axis therefore denotes the same month out of the 30-year period in each plot.) For short wave radiation a significant amount of scatter is obvious. However there is also a clear trend

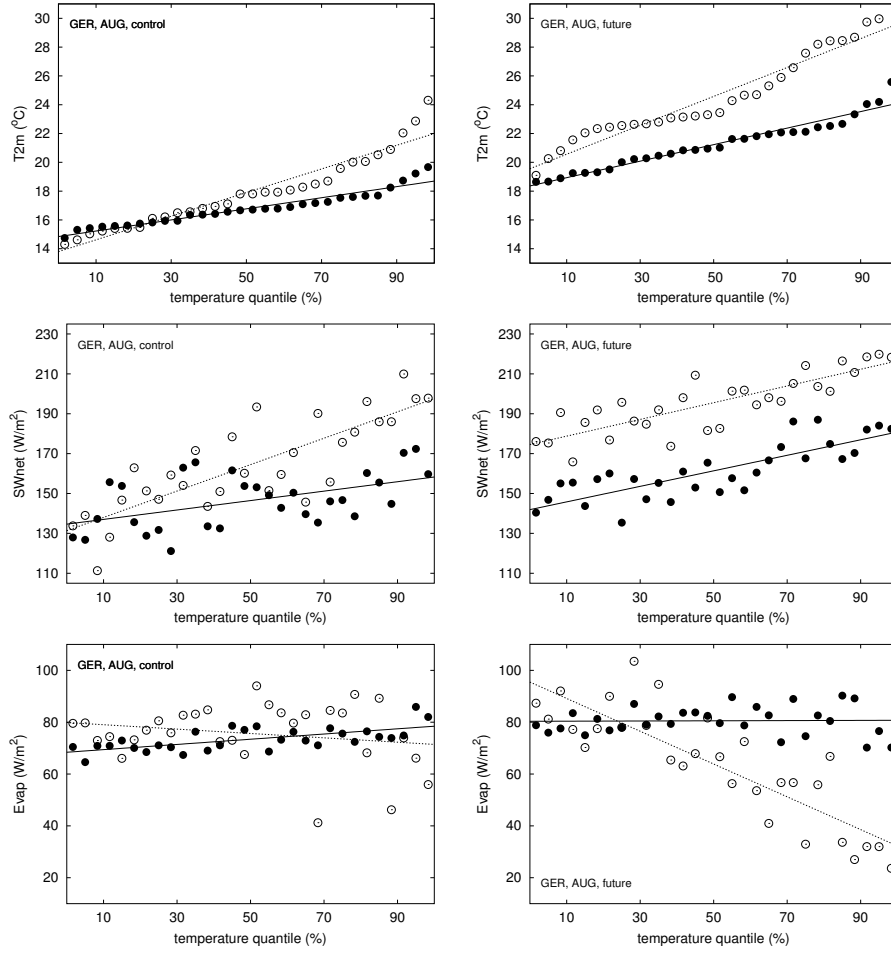


Figure 4. Scatter plots of area averaged (for area GER in August) mean temperatures, net short-wave radiation and evaporation at the surface against temperature quantile (see text). Results are shown for RACMO2 (solid dots) and HadRM3H (open circles), both for the control (left-hand panels) and the future (right-hand panels) integration.

with, as expected, the highest amounts of short wave radiation occurring in the warmest months out of the 30-years period. Then, a straight line is fitted through the data using a least squares fit, and the difference between the value of the fit at the 100% quantile with the value at the 0% quantile is defined as ΔSWnet . Similar definitions are used for the other terms in the surface energy budget; e.g. Δevap for evaporation. The same definition is also used for temperature variability, computing Δt_{2m} from a fit through the sorted temperature data; Δt_{2m} is about 3.3 times the standard deviation in all RCMs for each area and each summer month.

Figure 4 illustrates the typical differences in the model ensemble by showing some detailed results for two RCMs: RACMO2 and HadRM3H. For the

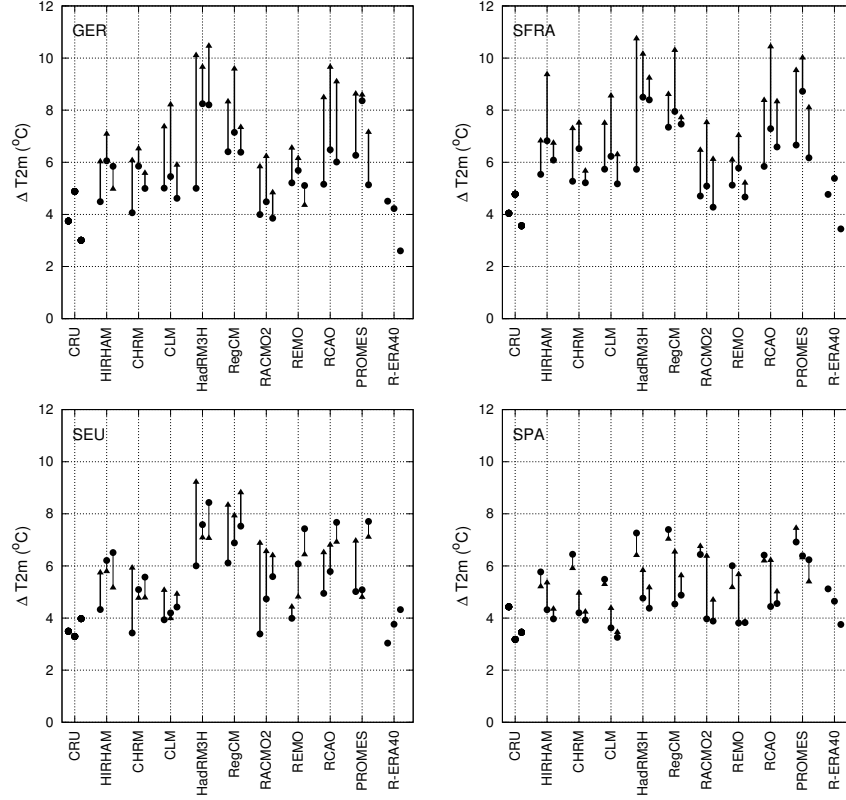


Figure 5. Panels of ΔT_{2m} for GER, SFRA, SEU, and SPA for each RCM integration, and the CRU observation (lines and symbols as Fig. 3)

control simulation ΔSW_{net} in HadRM3H is much larger than in RACMO2, and therefore short wave radiation contributes stronger to the temperature variability in HadRM3H than in RACMO2. For evaporation the slope of the fit for RACMO2 is positive – signifying higher evaporation rates in warm August months than in cold August months – and therefore evaporation acts to reduce the temperature variability. In HadRM3H the slope is negative, and evaporation therefore contributes to the temperature variability. The future integration shows an increase in mean short-wave radiation in both models, but ΔSW_{net} increases in RACMO2 and decreases in HadRM3H. Evaporation shows a very strong response in HadRM3H, with almost no evaporation in the warm months, and almost no response in RACMO2. Thus, in RACMO2 variability in short wave radiation contributes to the increased temperature variability, while in HadRM3H the contribution of the change in evaporation is dominant.

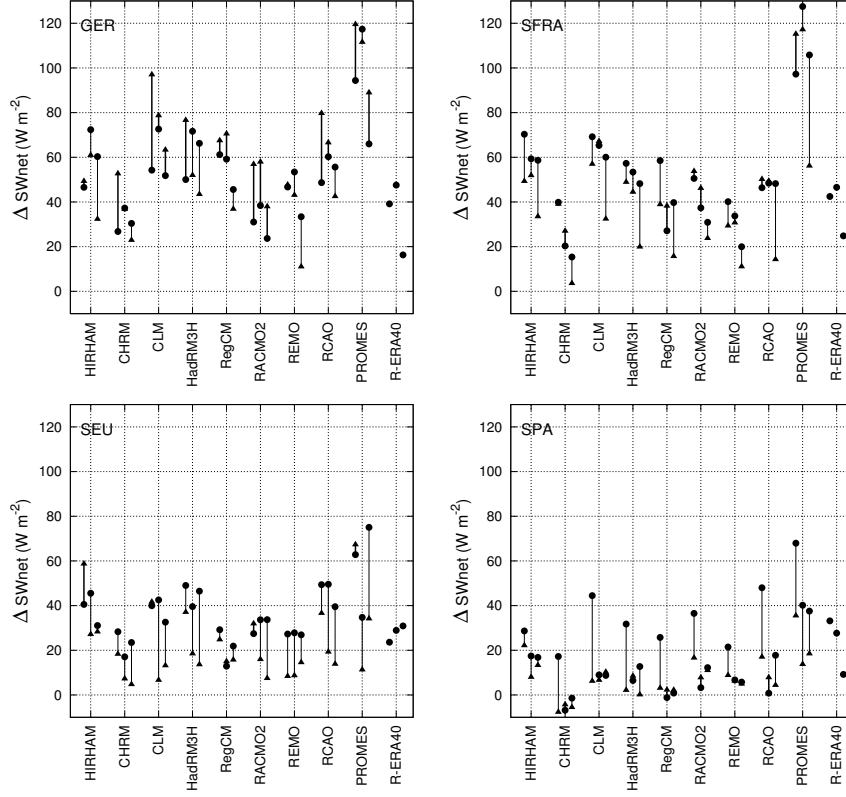


Figure 6. As Fig. 5, but now for ΔSWnet (no observations)

3.3. THE CONTROL PERIOD

We applied this methodology first to the surface fluxes of net short wave radiation, downward long wave radiation, and evaporation. We studied these terms because we expect the major differences in the parameterization of the RCMs in the representation of clouds and the cloud-radiation interaction, and the representation of the hydrological cycle and soil moisture, and these differences impact directly on these fluxes. Figures 5-8 shows Δt_{2m} , ΔSWnet , Δevap , and ΔLWdown for each summer month and each area defined, both for the control simulation as for the future simulation. For evaporation we plotted $-\Delta\text{evap}$ in order to have the same sign convention for each term; that is, positive values contributing to the temperature variability. Admittedly, these figures contain an overwhelming amount of data, and in the following we only highlight the most important findings.

There are large differences in simulated short-wave radiation among the different RCMs: in particular for SFRA and GER, ΔSWnet ranges from 20 to 100 Wm^{-2} . The high temperature variability in PROMES as shown in Fig. 5 appears to be related to the large variability in short wave radiation (Fig. 6).

Table II. Evaluation of net Short-wave radiation (Wm^{-2}) at De Bilt

	Jun mean	Jun delta	Jul mean	Jul delta	Aug mean	Aug delta
OBS. 1961-1990	174	48	159	50	141	27
OBS. 1973-2003	171	60	159	62	141	36
HIRHAM	187	38	195	67	162	61
CHRM	200	14	196	49	165	30
CLM	159	57	148	82	120	54
HadRM3H	195	52	189	87	158	59
RegCM	231	51	223	61	188	55
RACMO2	183	34	174	50	145	32
REMO	199	39	192	48	156	32
RCAO	181	38	170	74	144	57
PROMES	110	86	102	126	79	52
R-ERA40	179	53	168	59	136	18

CHRM and RACMO2 have rather low values of $\Delta\text{SW}_{\text{net}}$, and the behavior of the other models is in-between. All models show a decrease in $\Delta\text{SW}_{\text{net}}$ from GER and SFRA to SEU and SPA, showing that the influence of clouds on the radiative budget is larger in central Europe than in southern Europe.

A comparison with observations of short-wave radiation in De Bilt (The Netherlands) is summarized in Table 2. Net short-wave radiation is computed from global downward radiation using an albedo of 15 %. From the observations we calculated $\Delta\text{SW}_{\text{net}}$ to be between 48 and 62 in June and July (depending on the control period considered), and around 30 in August. Compared to these values PROMES clearly overestimates $\Delta\text{SW}_{\text{net}}$ in all summer months. Except CHRM, RACMO2 and REMO, most RCMs tend to overestimate $\Delta\text{SW}_{\text{net}}$ in July and/or August. On the other hand, CHRM, and to a lesser extent RACMO2, REMO and RCAO, appear to underestimate $\Delta\text{SW}_{\text{net}}$ in June.

Figure 7 shows the impact of soil drying on evaporation. For the relative moist conditions in GER the majority of the RCMs reveal no signs of reduced evaporation by soil moisture depletion, which is reflected by the positive values of Δevap . Thus evaporation acts to reduce temperature variability. Exceptions are August in HadRM3H and all summer months in CLM. The dryer conditions in SFRA lead to a much larger model spread, with some models sustaining high evaporation in the warm months (PROMES, REMO and RACMO2) relative to the evaporation in cold months, whereas others clearly show the influence of the soil moisture depletion in warm months on evaporation. In SEU all models (except PROMES) again agree in predicting negative values of

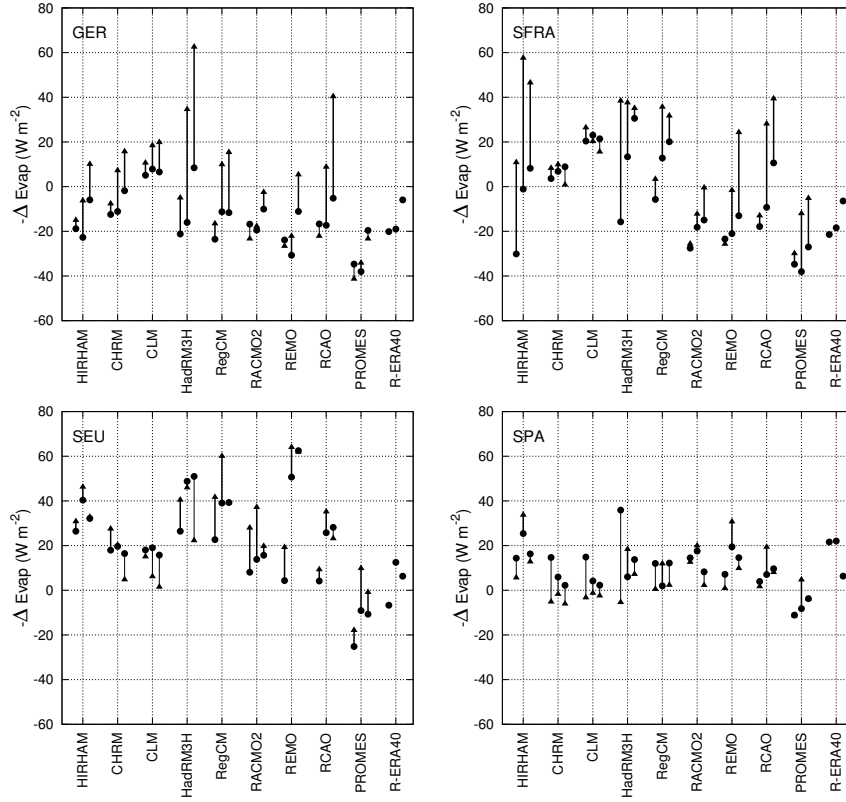


Figure 7. As Fig. 5, but now for $-\Delta\text{Evap}$ (no observations)

Δevap . Most models produce rather large negative values, therefore acting to enhance temperature variability significantly. Thus, SEU is characterized by a significant soil moisture control in all RCMs. Going further into the dry limit, all RCMs show smaller (and negative) values of Δevap in SPA. In the limit of a completely dry soil both mean evaporation and Δevap necessarily approach zero since there is no more moisture available for evaporation. In HadRM3H, for example, this explains the increase in Δevap from -38 Wm^{-2} in June, when the soil is not completely dried out yet, to close to zero in August.

The models results are rather consistent with respect to the downward long wave radiation (positive downward) as shown in Fig. 8, with values of ΔLWdown of $10\text{--}20 \text{ Wm}^{-2}$ for the majority of the models (HadRM3H not reported). Two models are outliers with values of ΔLWdown close to zero (PROMES and CLM), which is most likely caused by the strong cloud-radiation control in these models. Clouds act to increase the downward long wave radiation since they increase the effective radiative temperature of the atmosphere. Since warm months are associated with small amounts of clouds (and vice-versa), clouds cause a reduction of ΔLWdown . This strong-cloud radiation control is consistent with the results for short wave radiation for these models.

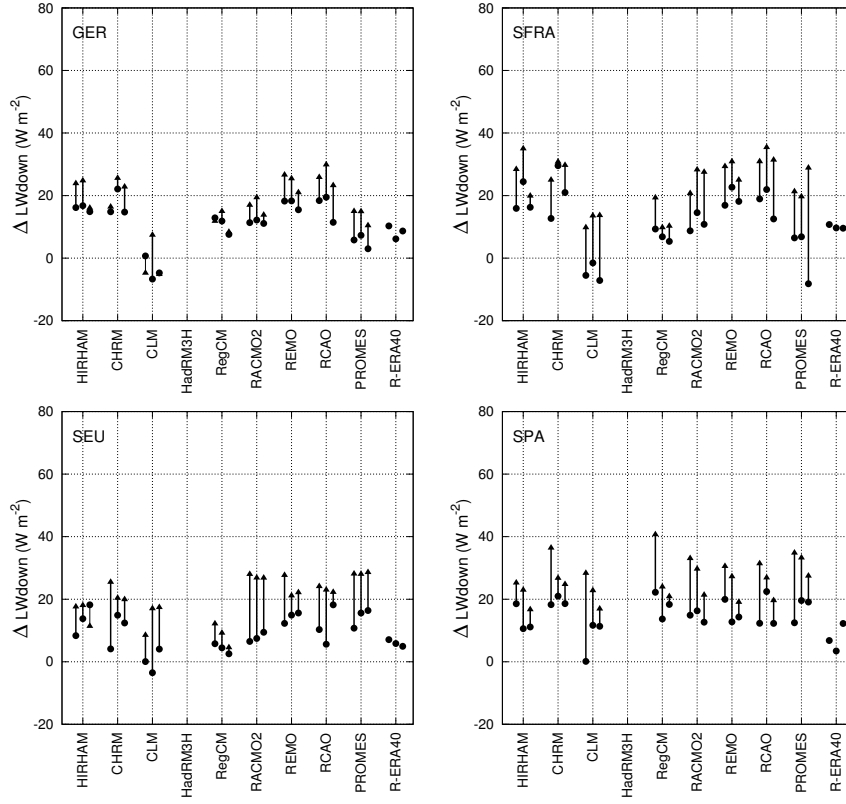


Figure 8. As Fig. 5, but now for ΔLW_{down} (no observations)

3.4. THE CLIMATE RESPONSE

Figures 5-8 also show the results for the future climate runs (triangles). In general, the temperature variability, as measured by Δt_{2m} , increases for each summer months and each area. For GER and SFRA the increase in temperature variability is significant in most models, but for SEU and SPA the increase is not as clear. For SEU the RCMs disagree, with some models predicting (almost) no increase (e.g. HIRHAM and CLM) and others predicting a large increase (e.g. RACMO2). In SPA the agreement between the different RCMs is larger, with most models predicting almost no increase in June and a small increase in July and August.

For SFRA and SEU most RCMs display a decrease of ΔSW_{net} from the control climate integration to the future integration. In GER the models diverge with some models predicting an increase (e.g. CLM and RACMO2) while others predicting a decrease (e.g. HIRHAM and RAO). In SPA ΔSW_{net} approaches zero, which is a manifestation of the fact that clouds are virtually absent (in the sense that they influence the radiative budget) in SPA even in “cold” months. The vast majority of the RCMs predicts an increase of the

contribution of evaporation to the temperature variability in GER and SFRA, but the magnitude varies considerably with values of the change in Δevap between close to zero and -40 Wm^{-2} . CLM has almost no response, and also the response in RACMO2 and PROMES is relatively small. HIRHAM, RCAO and HadRM3H have relatively large responses. In particular, the large response in June in HadRM3H in SFRA shows that the drying out of the soil start to limit evaporation already in early in summer. It is worthwhile noting that this corresponds to the large increase in temperature variability for June in HadRM3H. For SPA and SEU the response of Δevap is in general small. For SPA this mainly reflects that the models are close to their wilting points, and have very low mean evaporation (the mean evaporation as shown in Fig. 3 varies between 20 and 60 Wm^{-2} in most RCMs). Finally, for each area and each summer month ΔLWdown increases (see Fig. 8). The increase is largest for southern Europe (areas SPA and SEU). There is a large agreement between the different RCMs, except PROMES which shows a significantly larger response for SFRA, and CLM which (still) shows very low values for GER compared to the other models.

4. Surface energy budget and temperature variability

In order to be able to tie differences in surface fluxes to differences in the temperature variability, we focus on the surface energy budget which for this purpose we write as:

$$LW_{up} + H + G = LW_{down} + SW_{net} - LE \equiv F \quad (1)$$

with H sensible heat flux, LE the latent heat flux (evaporation), and G the soil heat flux, and LW_{down} , LW_{up} and SW_{net} the fluxes of downward long-wave, upward long-wave and net short-wave radiation, respectively. In this equation, we deliberately separated the terms which are strongly and physically dependent on the surface temperature on the left hand side from the other terms which have a weaker dependency on the surface temperature or are constrained by other quantities (e.g. soil moisture or atmospheric humidity in the case of evaporation). The sum of the terms on the right-hand side defines F . Obviously this separation is not a very strict separation, but if for the moment we accept it, we expect a scaling of the surface temperature variability on the variability in F . This follows from writing the equation as $R(T_s) = F$, with $R(T_s)$ a function of the surface temperature determined by the terms on the left-hand side, linearizing this function R around the 30-year mean temperature, and assuming that F is independent on the surface temperature.

Figure 9 shows the relation between temperature variability Δt_{2m} and ΔF (combining ΔSW_{net} , $\Delta Evap$ and ΔLW_{down}) for the areas SFRA and GER. In the model ensemble, there is a clear relation between surface forcing ΔF and the temperature variability. This holds for both the control and the future

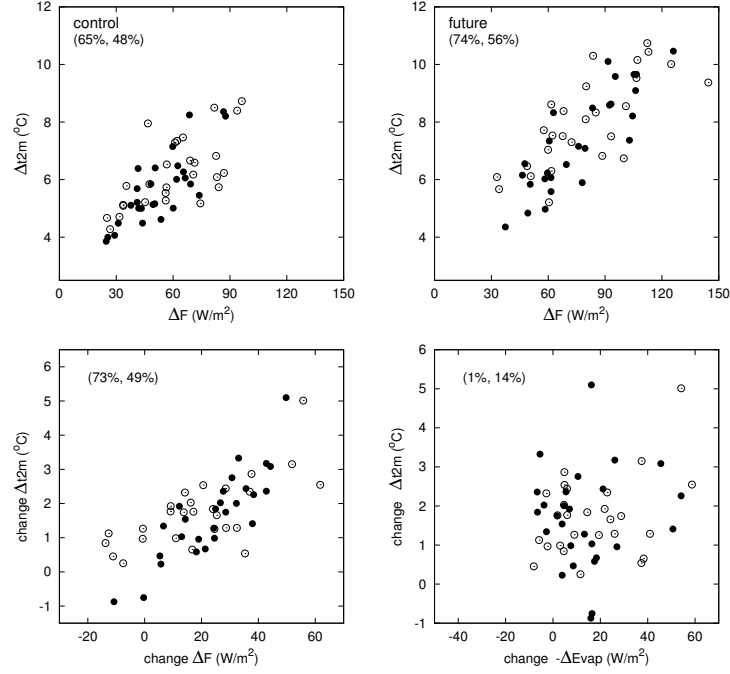


Figure 9. Scatter plot of temperature variability Δt_{2m} against $\Delta F = \Delta SW_{net} - \Delta evap + \Delta LW_{down}$, for the (a) control integration, and the (b) future integration. Change in temperature variability ($A2 - \text{Control}$) against (c) change in ΔF and (d) change in $\Delta Evap$. Results are shown for all models and each summer month for SFRA (open circles) and GER (dots). For HadRM3H we set ΔLW_{down} to the mean of the model ensemble. Numbers between parentheses denote the explained variance (%) of a linear regression of the data for (GER,SFRA)

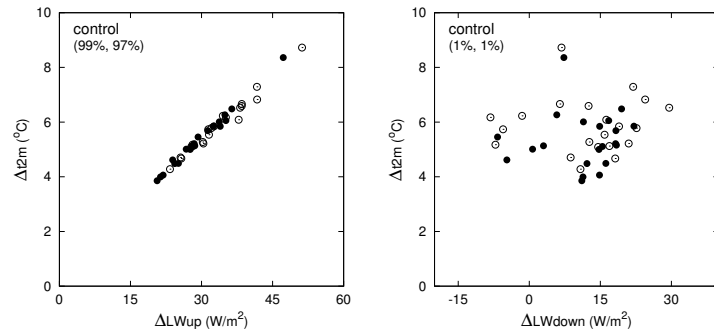


Figure 10. Panels of Δt_{2m} against ΔLW_{up} (a) and ΔLW_{down} (b) for the control simulation. Results are shown for all models, except HadRM3H (not available) and RegCM (data appear unreliable) and each summer month for SFRA (open circles) and GER (dots).

climate simulation separately, but also for the changes between control and future simulation. The explained variance is between 50-70 %, with in general the highest values for GER. For both areas the surface forcing ΔF increase from the control to the future simulation. For GER the slope of a linear fit between surface forcing and temperature variability is almost constant, ranging between $0.06 \text{ K (Wm}^{-2})^{-1}$ for both control and future simulation and $0.075 \text{ K (Wm}^{-2})^{-1}$ for the climate response. The slope may be used to estimate the contribution of the individual components, such as Δevap and ΔSWnet , to the temperature response. Fig. 9d shows that the change in Δevap does not correlate well with the change in temperature variability. The same applies to the change in ΔSWnet (not shown). However, the sum of short wave radiation and evaporation correlates much better. The results are close to Fig. 9c, shifted by $10\text{-}20 \text{ Wm}^{-2}$ to the left, and with slightly more scatter. Apparently, those models that have a weak response in evaporation are also characterized by a strong response the short wave radiation and vice-versa (as is e.g. illustrated for HadRM3H and RACMO2 in Fig. 4).

Admittedly, the above separation of the surface energy budget is based on a rather intuitive separation between “forcing” terms (contained in ΔF) and closure terms. However, we could also interpret ΔF simply as a predictor of the temperature variability. Then, the scatter and the offset (value of a fit through the data at $\Delta F = 0$) in Fig. 9a,b is a measure of the quality of our predictor. It is clear that including all terms of the surface energy budget in F makes a bad predictor, since these terms add up to zero by definition. Conversely, an almost perfect “predictor” is obtained by using the upward long wave radiation only. In the model ensemble, ΔLWup is highly correlated with Δt_{2m} , as shown in Fig. 10 for the control simulation. A fit through these data points gives a slope of $6 \text{ Wm}^{-2} \text{ K}^{-1}$, which is very close to the value obtained from the Stephan-Boltzmann radiation law. However, the upward long wave radiation flux is a consequence of the surface temperature. Therefore, it is a manifestation of the differences rather than that it explains the inter-model differences.

On the one hand, our forcing function F gives reasonable results in terms of scatter and offset. On the other hand, it provides a reasonable explanation in the sense that F is determined (at least to a significant extent) by processes not directly related to the surface temperature itself (external controls). For short-wave radiation and evaporation this is clear. However, for the downward long wave radiation this may not be so clear. The downward long wave radiation is determined for a significant part by the atmospheric boundary layer temperature, which is strongly tied to the surface temperature. Nevertheless, in the model ensemble there is no direct relation between temperature variability and ΔLWdown , as shown in Fig. 10. It therefore appears that other factors (like e.g. the presence or absence of clouds) contribute significantly to the spread in ΔLWdown .

Finally, it is noted that the sensible heat flux is a difficult term to interpret in this framework because it is related to the temperature *difference* between

the surface and the atmosphere. This means that part of it could be considered as a forcing term of the surface temperature: a positive atmospheric temperature perturbation (e.g. due to advection of warmer air) forces a higher surface temperature since it causes an initial reduction of the (upward) sensible heat flux, after which the surface adjust to a higher temperature state. Although mathematically we could try to separate the sensible heat flux into two contributions, with the forcing part related to the atmospheric temperature added to F , for practical reasons this was not feasible in this study. Nevertheless, we think that the sensible heat flux could explain part of the offset in Fig. 9a,b.

5. Discussion

5.1. CIRCULATION, LAND-SEA TEMPERATURE CONTRAST AND THE SURFACE ENERGY BUDGET

The analysis described above gives insight in the contributions of different terms in the surface energy budget to the temperature variability. A further analysis showed that a large part of the surface fluxes are (highly) correlated with the circulation (not presented). For example, the short wave radiation is highly correlated with the circulation with westerly flows bringing cloudy and easterly flows bringing cloud-free conditions. For evaporation this relation is not so clear. Easterly winds bring dry, warm, and sunny conditions thereby enhancing evaporation, but prolonged easterly winds may cause a drying out of the soil that reduces evaporation. The advection of warm air from the continent causes an increase in the downward long wave radiation flux; however, the reduced cloud cover that is associated may lead to a decrease in long wave radiative flux.

Increased mean surface radiation and decreased evaporation (see Fig. 3) cause high temperatures over the continent in the future climate, whereas Atlantic sea surface temperature increases are moderate. The resulting enhanced land-sea temperature contrast increases the dependency of the different surface energy budget terms on the circulation. In particular, the downward long wave radiative and the sensible heat flux are directly affected leading to higher variability, but also evaporation (higher moisture deficit between atmosphere and the soil) and cloud fields may respond strongly to the enhanced land-sea temperature contrast.

5.2. SENSITIVITY TO CIRCULATION BIASES

In Van Ulden et al. (2005) it is shown that the HadAM3H simulation is characterized by a too weak mean westerly flow in summer, but the variability around this mean flow appears realistic. To estimate the potential influence of these deviations in circulation statistics we briefly present results of the

RACMO2 model driven by analysis of the ERA-40 project. The results (period 1961-1990) are shown in Figs. 5-8, and table 2, labeled with R-ERA40. In general, the differences in Δt_{2m} between the two simulations are smaller than 1 °C. The inter-annual variability in both RACMO2 runs is (very) close to the observations. The differences in the surface fluxes are also not large. It is noted that for mean temperature the results are also similar except for south-eastern part of the domain. Temperature obtained with ERA-40 boundaries are 1-2 °C lower than those obtained with the HadAM3H boundaries. These results suggests that the bias in the circulation statistics in the HadAM3H boundaries is not a critical issue here. But one should be careful not to over interpret these results since the RACMO2 model has a rather large soil moisture capacity (Van den Hurk et al., 2005) and might therefore be rather insensitive to a mean easterly bias in the circulation.

5.3. MODEL CHARACTERISTICS

Specific model characteristics are summarized in terms of the relative behavior of the model considered compared to the ensemble mean. These characteristics are inferred mainly from the model results for central Europe (areas GER and SFRA). PROMES and to a lesser degree CLM, HIRHAM and HadRM3H are characterized by relatively large values of ΔSW_{net} , reflecting a large influence of clouds on radiation. This might be caused by both the amount of clouds simulated and the radiative properties of these clouds. Conversely, in CHRM and to a lesser degree RACMO2 the impact of clouds on radiation appears rather small. HadRM3H, and to a lesser degree HIRHAM, CLM, RegCM, and RCAO are characterized by relatively large negative values of $\Delta evap$, which can be attributed to a large sensitivity of the model to soil drying. RACMO2, PROMES and REMO, however, appear rather insensitive to soil drying, but we note that mean evaporation in PROMES is rather low. Finally, it is worth mentioning that despite that $\Delta evap$ in CHRM is not particularly large, the model has a considerable reduction of mean evaporation from the control to the future integration in SFRA, suggesting a significant soil moisture control on evaporation.

It is important to note that in the models the above characteristics for evaporation and short wave radiation are not independent. For example, in HadRM3H relatively high evaporation rates and high short-wave radiation during early summer cause a higher sensitivity of the model to soil drying during late summer. On the other extreme, (very) low short wave radiative fluxes (see e.g. table 2) and low evaporation rates in PROMES leave the model rather insensitive to soil drying, despite that this model appears to have rather small soil water storage capacity (Van den Hurk et al., 2005). Also soil drying has an impact on clouds and short wave radiation. A strong drying out of the soil in southeastern Europe may cause relatively high values of ΔSW_{net} in

central Europe, as appears discernible for the models sensitive to drying for GER in August.

6. Conclusions

The temperature variability of monthly mean temperatures in summer in an ensemble of nine different RCMs driven by boundaries of the HadAM3H model is studied for both for the control climate (1961-1990) and a future climate (2071-2100, using the SRES A2 emission scenario). The temperature variability in the control simulation of most (but not all) RCMs is significantly overestimated in Central Europe, in some RCMs up to 50-100 %, compared to the CRU TS2 2.0 observational data set (New et al., 2000). A run with re-analysed boundaries of one RCM (RACMO2) shows that the use of HadAM3H boundaries is not likely to be a major cause for the overestimation of the temperature variability, although it may contribute to some extent.

An analysis of the surface energy budget and its relation with the temperature variability is presented. A reasonable relation between the sum of net short wave radiation, downward long wave radiation, and evaporation, on the one hand, and temperature variability, on the other hand, could be established in the model ensemble (see Fig. 9). For the control integration, there are large differences in how much short wave radiation contributes to the temperature variability, with values of the surface forcing differing a factor five in Germany in France. For evaporation, most RCMs agree in Spain, and Germany, but disagree rather strongly in the intermediate areas, in particular for southern France. The modelled fluxes of evaporation and short wave radiation appear to be the main contributors to the overestimation of the temperature variability.

The temperature variability increases from the control to the future simulation. This increase is particularly large for central Europe (areas GER and SFRA), and smaller for areas in southern Europe (SEU and SPA). In general, the drying out the soil leads to a increased contribution of evaporation to the temperature variability, although there is a considerable spread between the models. The corresponding signal for short wave radiation is not so clear, and depending on the model it may act to enhance or reduce temperature variability, although in central Europe on average the effect is positive. In all models, the change in downward long-wave radiation contributes to the increase in temperature variability. The latter is likely due to combined effects of the larger land-sea temperature contrast and decreased cloud coverage in the future simulation.

We note that the model characteristics found appear also to be reflected in an analysis of daily maximum temperatures in summer (Kjellström et al., 2005). For example, in HadRM3H very high daily maximum temperature extremes occur for central Europe, whereas PROMES and CLM show the opposite behavior.

Finally, we would like to emphasize that our results basically reflect that the climate of central Europe is critically dependent on the water and energy budget. In this respect, this study should not be (primarily) considered as a quality assessment of the models, but merely an evaluation of the uncertainty given present-day, state-of-the-art representations of the water and energy budgets. Given the sensitivity of the climate system in central Europe, the added value of a multi-model ensemble is evident. In order to improve and validate models specific studies focusing on the energy and water budgets using observations are necessary, such as e.g. Van den Hurk et al. (2005) and Hagemann and Jacob (2005)

Acknowledgements

The authors would like to thank Olé Christensen, for collecting the RCM data used in this study, and Jens Christensen for leading PRUDENCE. Comments by D. Jacob, E. Kjellström, S. Hagemann, R. Jones, F. Giorgi and D. Rowell and two reviewers are acknowledged. The RCM data were obtained with financial support of the EU (Contract EVK2-2001-00156 PRUDENCE).

Appendix

The appendix contains quantile plots of mean temperature for the different areas. The quantiles are plotted for each month: JUN, JUL, and AUG. Model results are plotted as biases from the CRU observations.

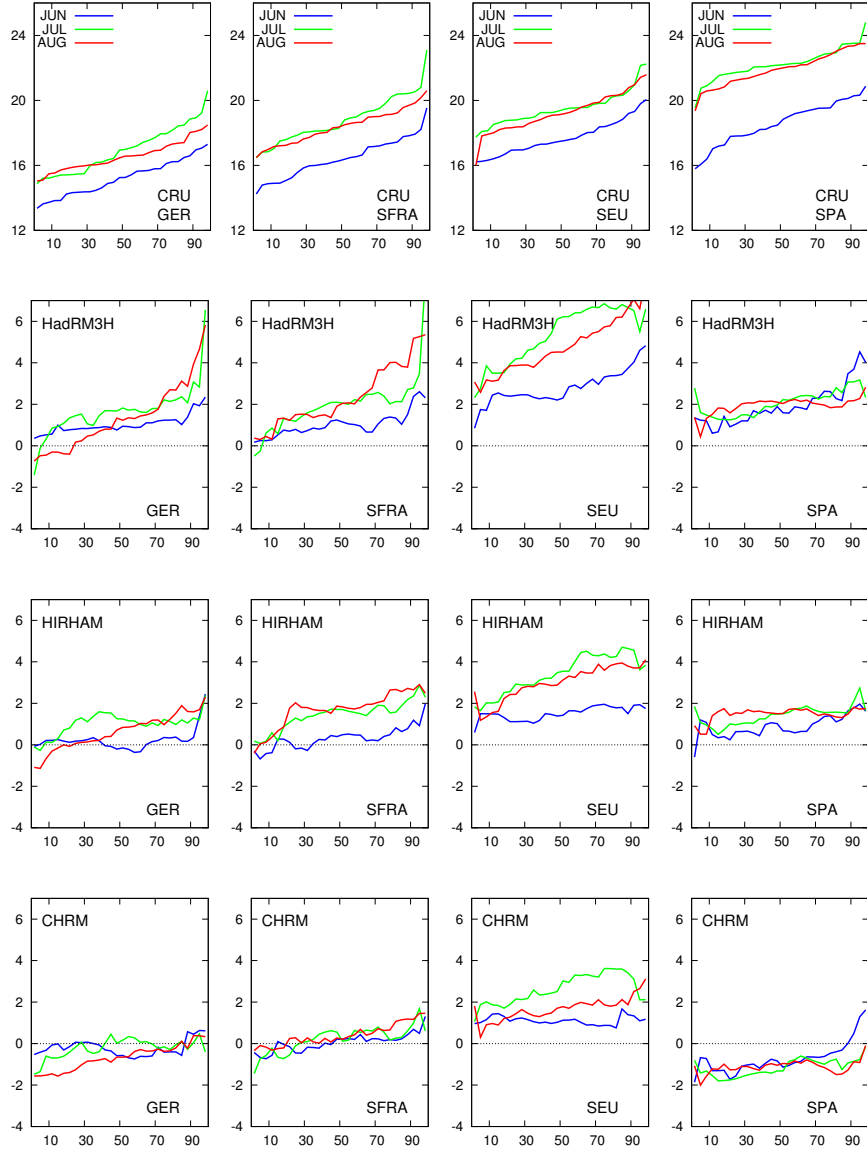
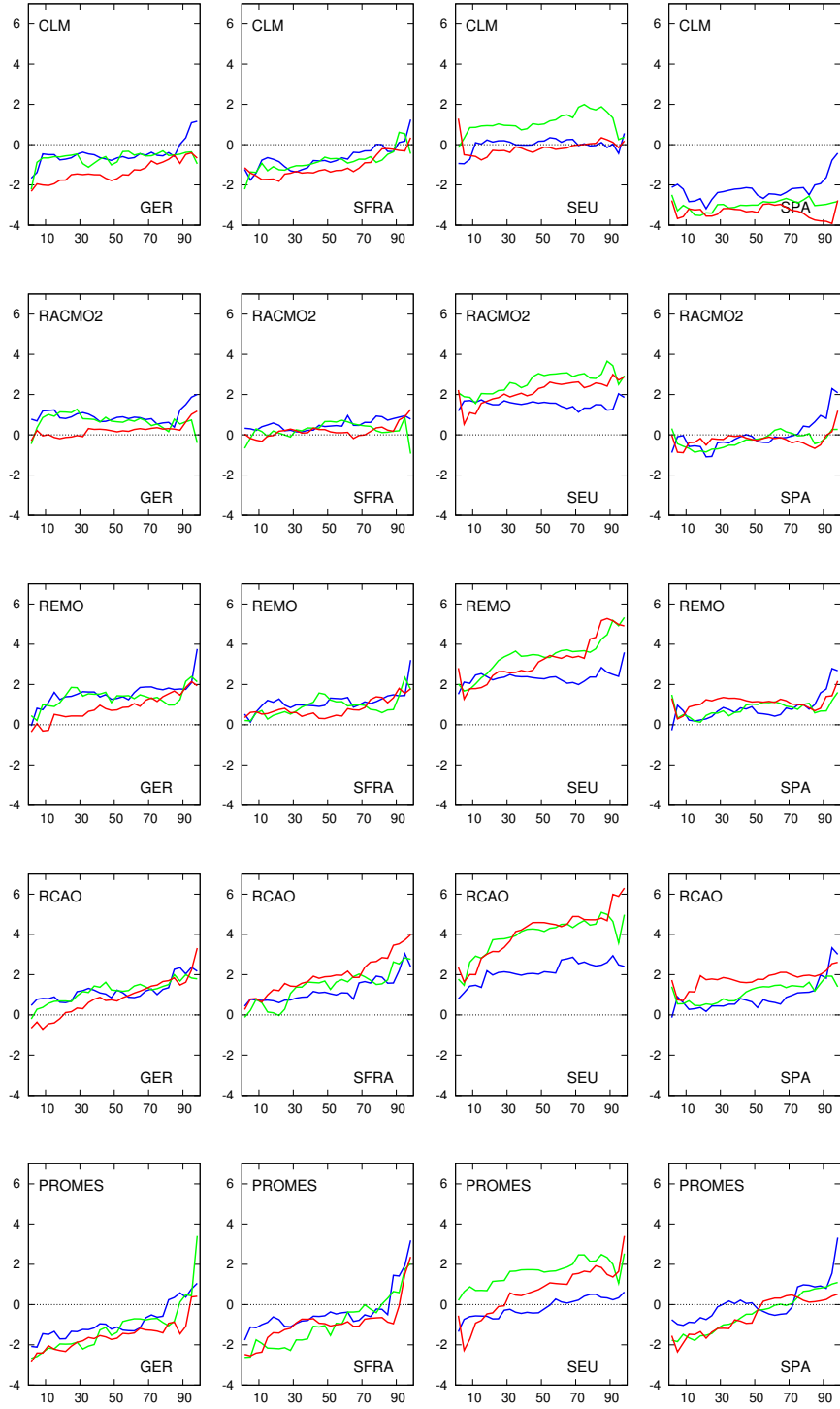


Figure 11. Quantile plots of monthly mean temperature for the different areas. Shown are the CRU observations (top panel) and the deviations from the CRU for the different RCMs (in °C)



(continued)

Figure 11.

References

- Beniston, M. and H. F. Diaz: 2004, 'The 2003 heat wave as an example of summers in a greenhouse climate? Observations and climate model simulations for Basel, Switzerland'. *Global and Planetary Change* **44**, 73–81.
- Christensen, J. H., T. R. Carter, and F. Giorgi: 2002, 'PRUDENCE Employs NEW Methods to Assess European Climate Change'. *EOS* **83**, 147.
- Christensen, J. H., O. Christensen, P. Lopez, E. van Meijgaard, and M. Botzet: 1996, 'The HIRHAM4 regional atmospheric climate model'. Technical Report 96-4, DMI.
- Giorgi, F., X. Bi, and J. Pal: 2004, 'Means, trends and interannual variability in a regional climate change experiment over Europe. Part I: Present day climate (1961-1990)'. *Climate Dynamics* **22**, 733–756.
- Giorgi, F. and L. O. Mearns: 1999, 'Introduction to special section: Regional climate modeling revisited.'. *J. Geophys. Res.* **104**, 6335–6352.
- Hagemann, S. and D. Jacob: 2005, 'Gradient in the climate change signal of European discharge predicted by a multi-model ensemble'. *Special issue Climatic Change* (accepted)
- Hulme, M., G. Jenkins, X. Lu, J. R. Turnpenny, T. D. Mitchell, R. G. Jones, J. Lowe, J. M. Murphy, D. Hassell, P. Boorman, R. McDonald, and S. Hill: 2002, 'Climate Change Scenarios for the United Kingdom: The UKCIP02 Scientific Report.'. Technical report, Tyndall Centre for Climate Change Research.
- Jacob, D.: 2001, 'A note to the simulation of the annual and inter-annual variability of the water budget of the Baltic Sea drainage basin'. *Meteor. Atm. Phys.* **77**, 61–73.
- Jones, R. G., J. M. Murphy, D. Hassell, and R. Taylor: 2001, 'Ensemble mean changes in a simulation of the European climate 2071-2100 using the new Hadley Centre regional modelling system HadAM3H/HadRM3H'. Technical report, Hadley Centre.
- Kjellström, E., L. Brring, D. Jacob, R. Jones, G. Lenderink, and C. Schär: 2005, 'Variability in daily maximum and minimum temperatures: Recent and future changes over Europe'. *Special issue Climatic Change* (accepted)
- Lenderink, G., B. van den Hurk, E. van Meijgaard, A. van Ulden, and H. Cuijpers: 2003, 'Simulation of present-day climate in RACMO2: first results and model developments'. Technical Report TR-252, Royal Netherlands Meteorological Institute.
- Luterbacher, J., D. Dietrich, E. Xoplaki, M. Grosjean, and H. Wanner: 2004, 'European Seasonal and Annual Temperature Variability, Trends and Extremes Since 1500'. *Science* **303**, 1499–1503.
- New, M., M. Hulme, and P. Jones: 2000, 'Representing Twentieth-Century Space-Time Climate Variability. Part II: Development of 1901-1996 Monthly Grids of Terrestrial Surface Climate'. *J. Climate* **13**, 2217–2238.
- Räisänen, J., U. Hansson, A. Ullerstig, R. Döscher, L. P. Graham, C. Jones, H. E. M. Meier, P. Samuelsson, and U. Willén: 2004, 'European climate in the late twenty-first century: regional simulations with two driving global models and two forcing scenarios'. *Climate Dynamics* **22**, 13–31.
- Sanchez, E., C. Gallardo, M. A. Gaertner, A. Arribas, and M. Castro: 2004, 'Future climate extreme events in the Mediterranean simulated by a regional climate model: a first approach'. *Global and Planetary Change* **44**, 163–180.
- Schär, C., P. L. Vidale, D. Lüthi, C. Frei, C. Häberli, M. A. Liniger, and C. Appenzeller: 2004, 'The role of increasing temperature variability in European summer heatwaves'. *Nature* **427**, 332–336 (doi:10.1038/nature02300).
- Seneviratne, S. I., J. S. Pal, E. A. B. Eltahir, and C. Schär: 2002, 'Summer dryness in a warmer climate: a process study with a regional climate model'. *Climate Dynamics* **20**, 69–85.

- Steppeler, J., G. Doms, U. Schättler, H. W. Bitzer, A. Gassmann, U. Damrath, and G. Gregoric: 2003, 'Meso-gamma scale forecasts using the nonhydrostatic model LM'. *Meteor. Atm. Phys.* **82**, 75–90.
- Van den Hurk, B., M. Hirschi, C. Schär, G. Lenderink, E. van Meijgaard, A. van Ulden, B. Rockel, S. Hagemann, P. Gahan, E. Kjellström, and R. Jones: 2005, 'Soil control on runoff response to climate change in regional climate model simulations'. *J. Climate* **18**, 3536–3551.
- Van Ulden, A., G. Lenderink, B. van den Hurk, and E. van Meijgaard: 2005, 'Circulation statistics in the PRUDENCE ensemble'. *Special issue Climatic Change* (accepted)
- Vidale, P. L., D. Lüthi, C. Frei, S. I. Seneviratne, and C. Schär: 2003, 'Predictability and uncertainty in a regional climate model'. *J. Geophys. Res.* **108** (D18), 4586 doi:10.1029/2002JD002810.
- Vidale, P. L., D. Lüthi, R. Wegmann, and C. Schär: 2005, 'European climate variability in a heterogeneous multi-model ensemble'. *Special issue Climatic Change* (accepted)

